Rain Rate and Modeled Fade Distributions at 20 GHz and 30 GHz Derived from Five Years of Network Rain Gauge Measurements

Julius Goldhirsh*, Vladimir Krichevsky#, Norman Gebo*
*The Johns Hopkins University, Applied Physics Laboratory
#Micromat Research, U.S.A.

Abstract

We examine five years of rain rate and modeled slant path attenuation distributions at 20 GHz and 30 GHz derived from a network of 10 tipping bucket rain gauges. The rain gauge network is located within a grid 70 km north-south and 47 km east-west in the Mid-Atlantic coast of the United States in the vicinity of Wallops Island, Virginia. Distributions were derived from the variable integration time data and from one minute averages. It was demonstrated that for realistic fade margins, the variable integration time results are adequate to estimate slant path attenuations at frequencies above 20 GHz using models which require one minute averages. An accurate empirical formula was developed to convert the variable integration time rain rates to one minute averages. Fade distributions at 20 GHz and 30 GHz were derived employing Crane's Global model because it was demonstrated to exhibit excellent accuracy with measured COMSTAR fades at 28.56 GHz.

1. Introduction

Earth-satellite communications at frequencies above 10 GHz suffer from attenuation caused by rain. Designers of such systems are interested in having a priori knowledge of the probability of exceeding different levels of rain attenuations so as to establish appropriate fade margins into their systems. They are also interested in establishing estimates of the year to year variability of rain fade margins for particular geographic regions so that communication systems reflect the extremes of these variabilities. Direct measurements of beacon signals from geostationary satellites have been a means to determine the above information [CCIR, 1986; Goldhirsh, 1982] and experiments are presently being pursued in Europe and the United States with satellites such as Intelsat [Vogel and Torrence, 1991] and Olympus [Satellite Communications Group, 1991], and in the near future with ACTS [Davarian, 1991]. Such measurements are also important for model development and validation.

The employment of rain-fade models is an ancillary approach for arriving at the above information. An important class of models use rain rate data acquired from rain gauges in different geographic regions for estimating cumulative distributions of slant path attenuation [CCIR, 1986]. Implementation of these models has the advantage that is relatively inexpensive, may be made over many years, and may address questions not easily addressed with

direct measurements; such as "What is the variability of fade distributions over distances of 10s of kilometers within a given geographic region?" and "What is the network average year to year variability in fades?" It is the objective of this paper to address the above questions through the presentation of analytical results of five years of rain rate data from a network of 10 rain gauges in the Mid-Atlantic coast of the United States. The results presented here is an expansion and elaboration of a previous effort by Goldhirsh [1990], encompassing two years of measurements.

Many slant path attenuation models employ one minute averages in their models [CCIR, 1986]. This creates a complication for investigators who utilize "tipping" bucket rain gauges because the rain rates are measured with variable integrations times. It is therefore another objective of this effort to assess the sensitivity to estimation errors of slant path attenuation distributions derived by variable integration times obtained from tipping bucket rain gauges. This question will be examined by comparing the variable integration time results with those derived employing one minute rain rate averages.

2.0 Description of Rain Gauge System

The rain gauges have an eight inch diameter collecting cylinder and contain buckets which tip after an accumulation of 0.254 mm of rainfall. After each tip, a switch at the gauge closes for approximately 100 milliseconds (switch closure time). The switch closure changes a voltage level monitored by a connecting PC. Whenever this voltage level change is noted, the PC records the computer clock time. Every two hours the accumulated tipping times are automatically recorded on files on a 5 1/4" disk. Also stored on the disk are the Julian date, the local time the file was written onto disk, and the total rainfall in mm.

The integration time ΔT (time between tips) is variable for the tipping bucket rain gauge and is defined by

$$R = \frac{914.4}{\Delta T} \qquad \text{(mm/h)} \tag{1}$$

where ΔT is expressed in seconds (integration time) and R is the rain rate in mm/h. We note that a 60 second integration time corresponds to a rain rate of 15.2 mm/h. Hence, measured rain rates smaller than approximately 15 minutes have integration times which are longer than one minute. A rain rate of 1 mm/h has an integration time of 15 minutes which represents approximately the lower measurement threshold with the above described gauge.

We report on the results of 10 rain gauges located within a gridded region of 70 km north-south and 47 km east-west in the Mid-Atlantic coast of the United States. All the gauges are located within a radial distance of 60 km from the SPANDAR radar facility at the NASA Goddard Wallops Flight Facility (WFF), Wallops Island, Virginia. The 10 gauge locations are depicted in the map of Figure 1. The individual rain gauge systems are located at the home grounds of staff working at the WFF. The staff maintains these systems on a continuous basis. The floppy disks are removed on a weekly basis and submitted to a central processor for reduction and analysis. Careful calibrations for each of the site gauges are performed twice per year and the system is maintained with errors of less than 5% in rain

rate at rates of 12 to 15 mm/h [Gebo, 1991].

3.0 Network Rain Rate Distributions

The rain rate distributions described in the following paragraphs were derived from measurements of 10 rain gauge sites encompassing the period June 1, 1986 through May 31, 1991 with the following caveats; the data related to Site #4 were only available for four years (June 1, 1987 through May 31, 1991), and the data for Site #6 for three years (June 1, 1986—May 31, 1989). The time and network average distributions were weighted to reflect the shorter operational time periods of these two sites.

3.1 Overall Average Rain Rate Distribution

In Figure 2 is plotted the combined distribution comprising the spatial (10 sites) and temporal (five years) average rain rate distributions for the variable integration time. Also plotted for comparison is the one minute integration time case. The combined average will hereafter be referred to as the "overall average" case. The one minute distribution was obtained by averaging the variable rain rate–time series over one minute contiguous periods and determining the cumulative distributions for the one minute average rain rate–time series. These two rain rate distributions are noted to be different by less than 3 mm/h up to 60 mm/h (0.01 % probability) where the time between tips is approximately 15 seconds.

It was shown by the authors [Goldhirsh et al., 1992] that at the 0.05% level, the differences between the modeled attenuations derived from the variable integration time and the one minute average distributions are negligibly small at both 30 GHz (0.6 dB) and 20 GHz (0.3 dB) compared to the respective fade levels (31.1 dB and 13.8 dB). We therefore conclude that it is not required to use one minute averages in the modeled rain rates over the range of practical (modeled) fade margins at 20 GHz and 30 GHz.

3.2 Scaling Formulation–Rain Rate Distributions

For completeness, however, we address the question as to how one may scale the rain rate distributions obtained with the variable integration time gauge to distributions which correspond to one minute averages. This formulation may be used to assess attenuations at lower frequencies where higher rain rates may define realistic fade margins. Thereafter, rain rate and modeled attenuation distributions will be presented here which correspond only to the variable integration time rain rate results.

A formulation has been derived which converts the variable rain rate distributions to the one minute distributions in the percentage interval 0.1% to 0.001% [Goldhirsh et al., 1992]. At percentages greater than 0.1%, the distributions are virtually identical for the described rain gauge. The formulation is given by

$$R_1(P) = R_v(P) - \delta(P) \tag{2}$$

where

$$\delta(P) = \alpha + \beta R + \gamma R^2 \tag{3}$$

$$\begin{cases} \alpha = -\ 0.2036 \\ \beta = 2.250 \times 10^{-2} \\ \gamma = 4.729 \times 10^{-4} \end{cases} \tag{4}$$

and where $R_1(P)$ is the one minute averaged rain rate (mm/h), $R_v(P)$ is the variable integration time rain rate, and $\delta(P)$ is the correction factor given by (3) and (4). All of these quantities are taken at the probability, P. The above formulation predicts the 60 second "overall average" distribution to within 2.5 mm/h at the 0.001% level.

3.3 Temporal Variability–Rain Rate Distributions

To establish a measure of the year to year variability in the rain rate distributions, we show in Figure 3 five distributions corresponding to the network average for each of five years (1986-87, 87-88, 88-89, 89-90, 90-91; hereafter referred to as years 1 through 5, respectively). Also plotted (dotted curve) is the "overall average" distribution. We note from Figure 3 that four of the years for the network average show similar distributions and year 4 shows considerably larger rain rates. For example, at 0.1%, year 4 shows a rain rate of approximately 24 mm/h compared to a range of other rain rates between approximately 11 mm/h and 15 mm/h. This result is a demonstration of the need to obtain multi–year rain rate distributions in order to assess extreme levels that may arise. At the 0.1% level a maximum rain rate difference of 13 mm/h exists. This is the difference between values for year #4 (highest rain rate) and year #5 (lowest rain rate).

3.4 Spatial Variability–Rain Rate Distributions

In this section we examine the variability in the distributions caused by measurements at different locations separated by 10s of kilometers within the Mid-Atlantic coast geographic region. In Figure 4 is given the rain rate distributions for each of 10 sites averaged over the five year period; with the exception of Sites #6 and #4 averaged over 3 and 4 years, respectively. It is apparent that the variability in the distributions for the individual site locations (Figure 4) appears to be smaller than the year to year variability (Figure 3). The maximum rain rate differences at 0.1%, 0.01%, and 0.001% are 3.5, 12.2, and 18.0 mm/h, respectively. Shown also, (dotted curve) is the overall network and temporal average.

We observe from Figure 4 that Site #1 shows generally larger values, whereas Site #6 shows generally minimal levels of rain rates. Site #6 (Figure 1) is located closest to the shoreline, where the rains tend to diminish because of the cooling effects of the sea water. That is, the cooler sea water tends to dampen the more intense convective rain cells which originate over land and are sustained by ground heating, as for example, air mass type systems. Site #1 is the most northerly site located approximately 10 km from the shore but furthest from the Chesapeake Bay than the other sites. Storm systems, which are generally out of the south-west, will move over a greater land mass and be sustained by ground heating as they pass Site #1 as compared to the other sites.

4.0 Attenuation Distributions

4.1 Employment of the Global Model

We use here the Crane's Global model [Crane, 1980] to derive the corresponding attenuation distributions at 20 GHz and 30 GHz at a slant path elevation angle of 45°. This model was employed here because of it's success in estimating the COMSTAR derived attenuation distribution at 28.56 GHz [Goldhirsh, 1982] when applying the measured rain rate distribution [Goldhirsh, 1990; Goldhirsh et al, 1992]. A comparison between the directly measured

rived using the Global Model and the "overall average" network rain rates showed differences between the two curves of only 2 dB or less.

4.2 Temporal Variability–Attenuation Distributions

In Figures 5 and 6 are plotted the network averaged yearly attenuation distributions over the five year period for 20 GHz and 30 GHz, respectively. It is apparent that the relatively intense rain rates alluded to previously for year 4 has considerable impact on the

been demonstrated that at frequencies of 20 GHz and 30 GHz and at realistic fade margins,

Gebo, N., "Volumetric Calibration of the Mid-Atlantic Coast Rain Gauge Network," *APL/JHU Technical Report #S1R-91U-010* April 10, 1991.

Goldhirsh, J., V. Krichevsky, N. E. Gebo, "Rain Rate Statistics and Modeled Slant Path Fade Distributions at 20 GHz and 30 GHz Derived from a Rain Gauge Network in the Mid-Atlantic Coast of the United States over a Five Year Period," *APL/JHU Technical Report*, S1R92U-006, March, 1992.

Goldhirsh, J., "Spatial variability of rain rate and slant path attenuation distributions at 28 GHz in the Mid-Atlantic coast region of the United States," *IEEE Trans. Antennas Propagat.*, vol. AP-38, pp. 1711–1716, 1990.

Goldhirsh, J. "Slant path fade and rain rate statistics associated with the COMSTAR beacon at 28.56 GHz for Wallops Island, Virginia over a three year period," *IEEE Trans. Antennas Propagat.*, vol. AP-30, pp. 191–198, 1982.

Satellite Communications Group, "Communications and Propagation Experiments Using the Olympus Spacecraft; Report on the First Year of Data Collection," *Virginia Tech Report EESATCOM 91-4*, October, 1991. (Virginia Polytechnic Institute, Bradley Department of Electrical Engineering, Blacksburg, VA 24061.)

Vogel, W. J. and G. W. Torrence, "INTEL–5040B: Three Years of Low Elevation Angle, K_u Band Satellite Beacon and Radiometer Measurement Results for Austin, Texas," *Final Analysis Report from the Electrical Engineering Research Laboratory, The University of Texas* 25 September, 1991. (The University of Texas at Austin, 10,100 Burnet Road, Austin, TX 78758–4497.)

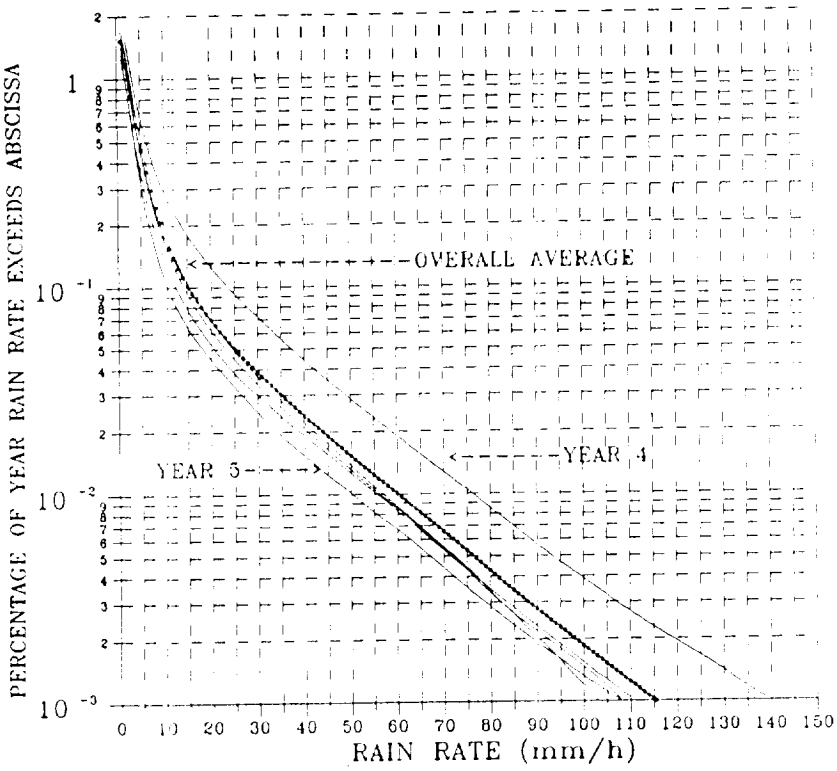

Figure 3: Comparison of yearly network average rain rate distributions over years 1 through 5.

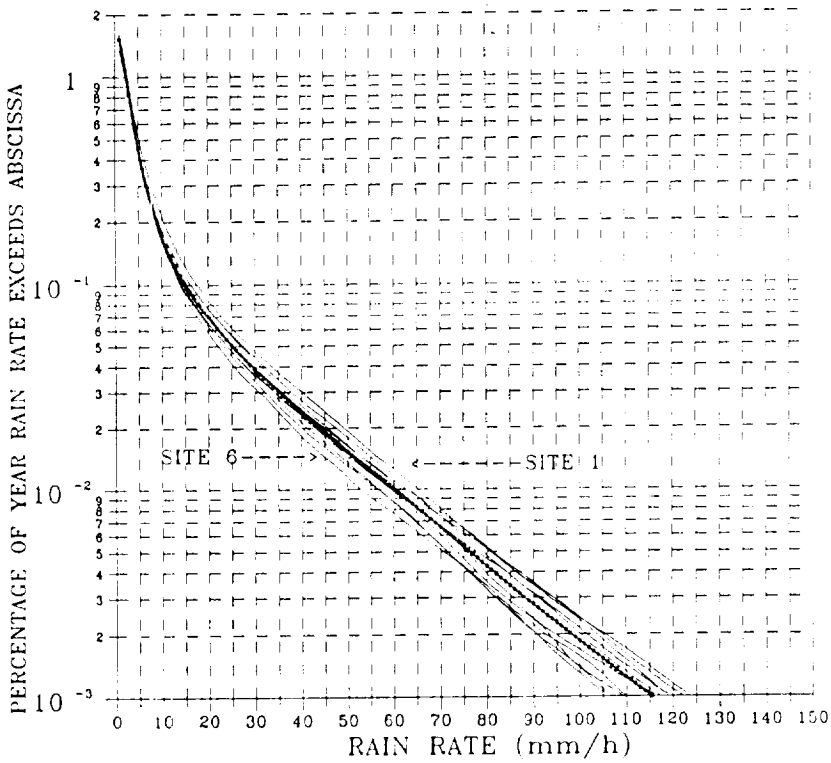

Figure 4: Comparison of rain rate distributions for 10 sites. Each site was averaged over five years with the exception of Site #6 (3 years) and Site #4 (4 years).

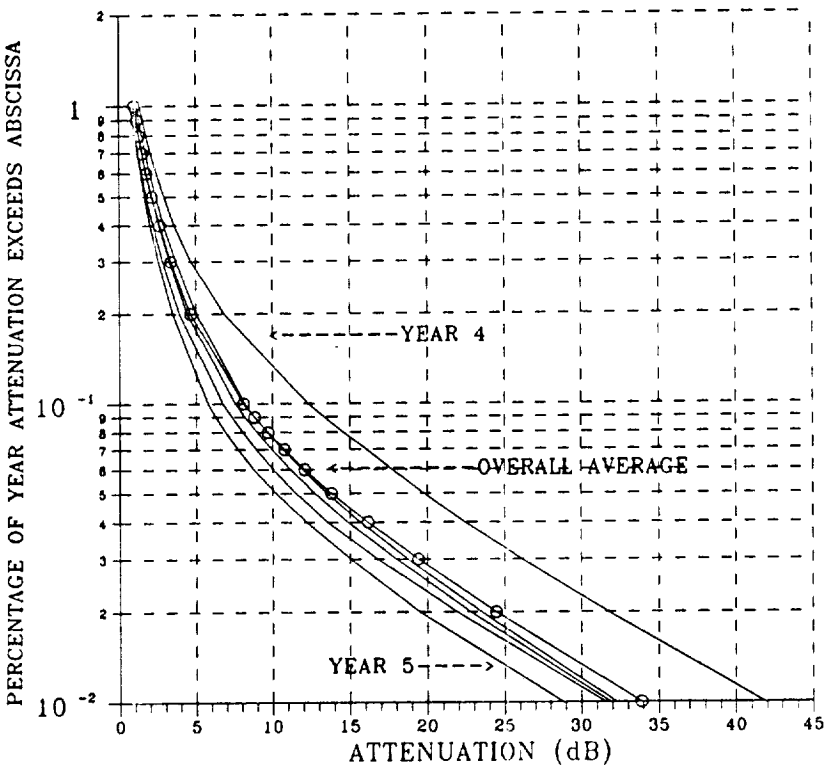

Figure 5: Comparison of yearly network average attenuation distributions at 20 GHz over years 1 through 5.

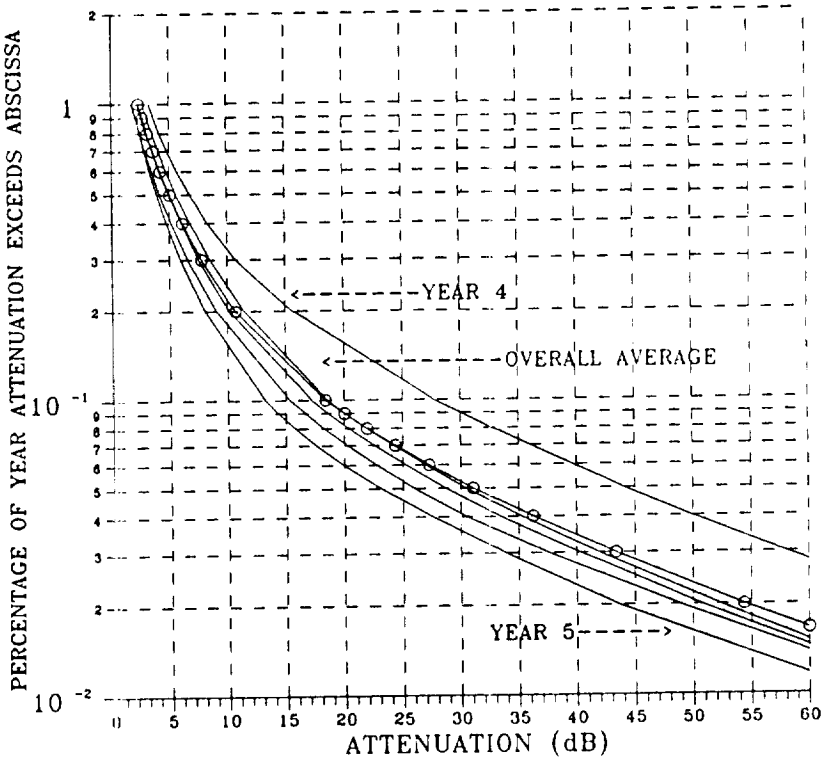

Figure 6: Comparison of yearly network average attenuation distributions at 30 GHz over years 1 through 5.

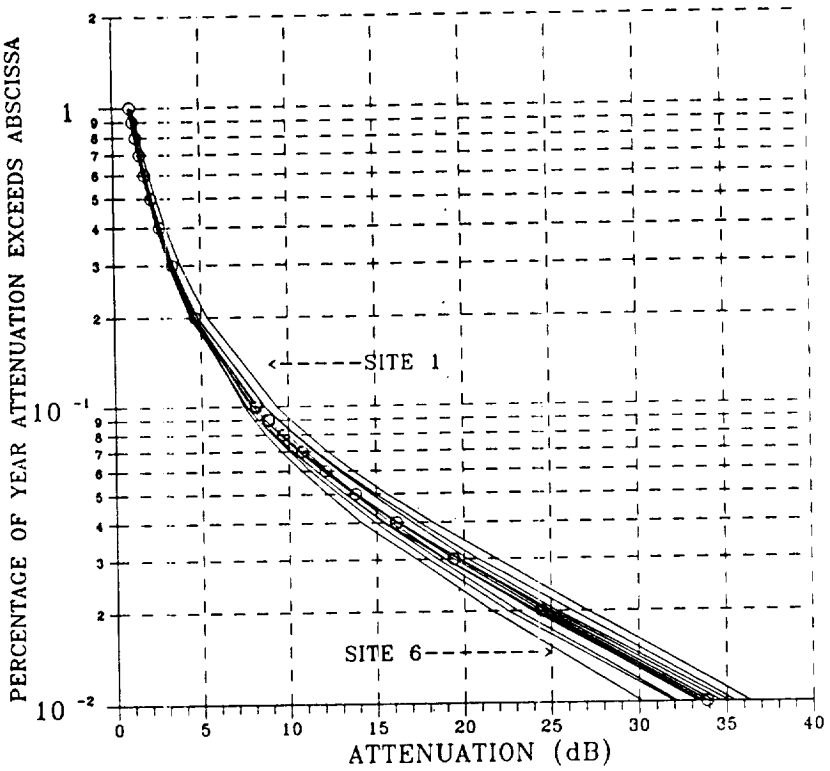

Figure 7: Comparison of attenuation distributions at 20 GHz for 10 sites. Each site was averaged over five years with the exception of Site #6 (3 years) and Site #4 (4 years).

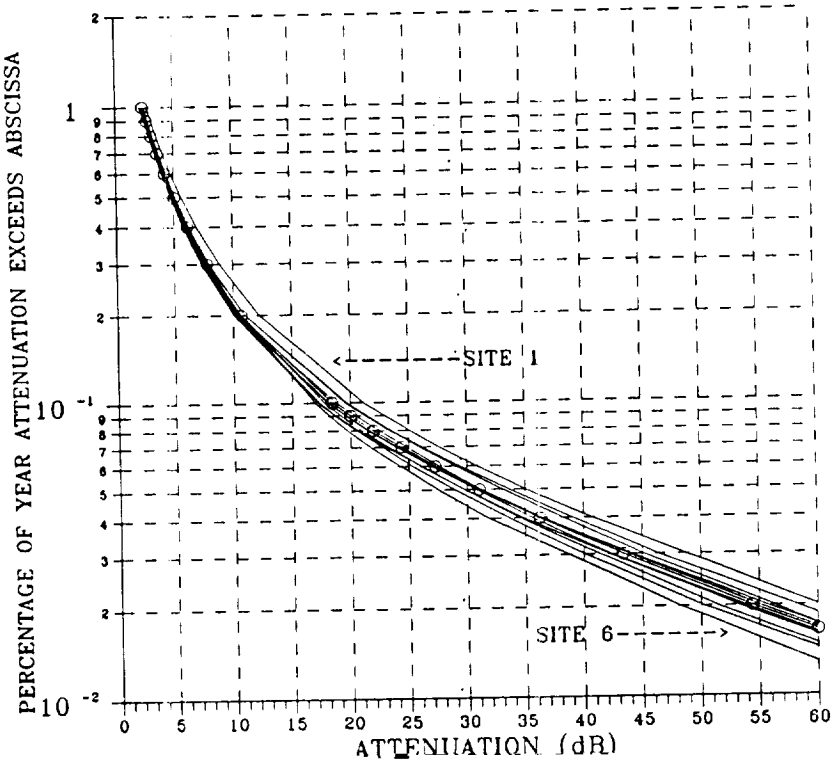

Figure 8: Comparison of attenuation distributions at 30 GHz for 10 sites. Each site was averaged over five years with the exception of Site #6 (3 years) and Site #4 (4 years).